International Journal of Hydrogen Energy 204 (2026) 153331

Contents lists available at ScienceDirect

International Journal of Hydrogen Energy

journal homepage: www.elsevier.com/locate/he

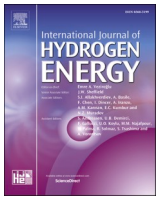

Efficient hydrogen storage in hydrate solid solution: Structural insights and performance

Siyuan Chen [a], Xinying Li [a], Yanhong Wang [a,c,*], Shuanshi Fan [a], Xuemei Lang [a,b], Hongfeng Lu [d], Gang Li [a]

[a] School of Chemistry and Chemical Engineering, South China University of Technology, Guangzhou, 510640, China
[b] Key Laboratory of Fuel Cell Technology of Guangdong Province, Guangzhou, 510640, China
[c] Key Laboratory of Heat and Mass Transfer and Low-Carbon Conversion, Ministry of Education, South China University of Technology, Guangzhou, 510640, China
[d] National Engineering Research Center of Gas Hydrate Exploration and Development, Guangzhou Marine Geological Survey, China Geological Survey, Guangzhou, 511458, China

ARTICLE INFO

Keywords:
Gas hydrate
Hydrogen storage
Solid solution
Lattice distortion
Raman spectrum

ABSTRACT

Clathrate hydrate is regarded as a quite promising functional material for energy storage. Here, we reported a conceptually innovative approach by constructing a hydrate solid solution through synergistic integration of sulfur hexafluoride (SF_6) and tetrabutylammonium bromide (TBAB). The lattice distortion of the new hydrogen-bonded framework was validated by PXRD and Raman spectroscopy. And DSC indicated TBAB/SF_6 hydrate solid solution exhibited excellent thermodynamic stability. The lattice distortion fundamentally alters cage dynamics, enabling unprecedented H_2 diffusion kinetics with the characteristic of two-step hydrate formation: A rapid storage stage achieved 0.453 wt% within 30 min, followed by a slow, constant-rate diffusion stage reaching 0.527 wt% over 8 h. The lattice distortion of TBAB/SF_6 hydrate solid solution facilitated hydrogen diffusion into the hydrate phase, while Raman analysis verified double H_2 occupancy in the small cages. The TBAB/SF_6 hydrate solid solution represents a tunable platform for efficient hydrogen storage. This work establishes that controlled lattice defects can be harnessed to optimize cage functionality.

1. Introduction

With the increasing global environmental challenges caused by the use of fossil fuels, hydrogen energy, as a clean energy carrier, is becoming more prominent [1]. The hydrogen energy industry chain mainly includes hydrogen production, storage, and utilization, among which hydrogen storage is currently the key factor for the commercial application of hydrogen energy. Conventional methods such as compression, liquefaction, adsorption, etc. partially face the problems of high energy consumption, difficulty of storage and transportation, and poor reversibility [2–4]. Hydrate-based hydrogen storage, as a newly developed technology, has attracted much attention as the characteristics of mild storage and transportation conditions, no pollution, and simple release process [5], and is regarded as the next generation hydrogen storage materials [6].

Clathrate hydrates are crystalline compounds with water molecules as the host, which generally exhibit different crystal structures (sI, sII, sH, and semi-clathrate), usually dictated by the size of the guest molecules [7]. And hydrate-based hydrogen storage can be achieved just by occupying the hydrate cages as guest molecules. Mao et al. [8,9] synthesized pure hydrogen hydrates at 2300 MPa and 300 K with the storage capacity of 11.2 wt%. Although the storage capacity was considerable, the formation conditions required were too harsh for industrial production. Florusse et al. [10] first suggested that thermodynamic additive (THF) could occupy the large cages to achieve stable storage of hydrogen molecules in the small cages at 279.6 K and 5 MPa. This discovery provided theoretical support for the commercial application of hydrate-based hydrogen storage technology, but the additives would occupy the large cages and fundamentally reduce the theoretical hydrogen storage capacity of hydrates (1.06 wt%) [11]. Even so, the experiment results have not achieved high hydrogen storage capacity under practical conditions, usually 0.2–0.6 wt% [12–14], only about half of the theoretical storage capacity. Fundamentally, the obstacle to achieve the theoretical hydrogen storage capacity is that the limited effective hydrate cages and mostly concentrated at the gas-solid interface, it is difficult for hydrogen molecules to enter the inner hydrate

* Corresponding author. School of Chemistry and Chemical Engineering, South China University of Technology, Guangzhou, 510640, China.
E-mail address: wyh@scut.edu.cn (Y. Wang).

https://doi.org/10.1016/j.ijhydene.2025.153331
Received 9 August 2025; Received in revised form 16 November 2025; Accepted 29 December 2025
Available online 31 December 2025

layer.

The formation of hydrogen hydrates is a complex process of heat transfer, mass transfer, and phase change. The key issue to improve the hydrogen storage capacity is to increase the number of "effective hydrogen cages" of hydrates, namely the hydrate cages that hydrogen molecules can enter. While the diffusion of hydrogen molecules into the hydrate cages is the key factor [15]. Wang et al. [16,17] indicated that hydrogen molecules can rapidly enter the cages of the outer hydrate layer with molecular dynamics simulations, but the occupied 5^{12} cages on the boundary layer would hinder further diffusion of hydrogen molecules into the inner hydrate layer; Hasegawa et al. [18] and Gorman et al. [19] also used molecular dynamics simulations to demonstrate that hydrogen molecules mainly diffused by the six-membered ring in the hydrate phase, and rather difficult to diffuse by the five-membered ring. However, thermodynamic additives would occupy the large cages, thereby affecting the diffusion of hydrogen molecules along the large cages in the hydrate phase and reducing the hydrogen storage capacity.

To improve the hydrogen storage capacity, the problem of the diffusion of hydrogen molecules into the bulk phase must be solved first. And the process of hydrogen diffusion within the hydrate bulk phase is related to the structural configuration and lattice defects of hydrates. The small cgaes (5^{12} cages) of structure sII hydrate formed a well-ordered barrier, while the $5^{12}6^4$ cages are occupied by thermodynamic additives, so hydrogen molecules cannot penetrate the 5^{12} cages into inner hydrate cages easily, hindering the diffusion of hydrogen molecules and causing a significant reduction in effective hydrogen cages, unless sufficient driving force. However, the 5^{12} cages of the semi-clathrate hydrates are not coherent as semi-clathrate hydrates are mainly composed of four super large cages [20]. Hydrogen molecules can easily penetrate from the large cages into the inner empty cages.

Based on the above ideas, we constructed a hydrate solid solution structure composed of sII and semi-clathrate hydrate cages. In this work, it was expected that the small cages of sII hydrates would serve as the main site for hydrogen storage, and the cages of semi-clathrate hydrate could provide the hydrogen diffusion channel for inner hydrate layer. Additionally, the combination of these two structures was beneficial for reducing the phase equilibrium conditions to increase the driving force. The thermodynamics, kinetics, and hydrogen storage performance of the hydrate solid solution were systematically studied, and the hydrogen occupancy behavior in this structure was analyzed and the corresponding mechanism was proposed.

2. Experimental

2.1. Materials

High purity SF_6 and H_2 were supplied by Foshan Kodi Gas Chemical Co., Ltd; Tetrabutylammonium bromide (TBAB) with a purity of 99.0 % was purchased from Beijing InnoChem Science & Technology Co., Ltd. The deionized water used for all the experiments was prepared in our laboratory. All reagents were used as received without further purification.

2.2. Apparatus

The schematic diagram of the experimental setup used to prepare and hydrogen storage performance of TBAB/SF_6 hydrate solid solution is shown in Fig. 1. The experimental setup includes a high-pressure stainless-steel cell with an internal effective volume of 300 mL, inner diameter of 50 mm, sidewall thickness of 8 mm, height of 153 mm. The cell is removable, the lid and the body are sealed by thread and fluorinated rubber O-ring, and a pressure sensor (Senex DG-1300, accuracy of ±0.25 %) and two platinum resistance thermometers (PT-100, accuracy of ±0.1K) are connected to the top of the hydrate formation cell to measure the pressure and temperature inside the cell, respectively. And the sensors are also connected to the data acquisition system (DAQ, Agilent 34970A) to collect and transfer the data to a computer, which records data every 10 s. A magnetic stirring device is at the bottom of the water bath. Gas chromatography (Kechuang GC 9800, TCD detector) was used to analyze the gas composition in the hydrate phase.

2.3. Procedures

In this work, the experimental procedures entailed two parts: Part 1-the kinetics and hydrogen storage performance of TBAB/SF_6 hydrate solid solution, and the hydrogen occupancy behavior in this structure. Part 2-the preparation of TBAB/SF_6 hydrate solid solution and blank hydrate samples (SF_6 hydrate and TBAB hydrates), Raman, DSC and PXRD were used to characterize the hydrate solid solution and illustrate the mechanism.

2.3.1. Kinetic experiments and Raman spectroscopy measurements

The formation kinetics and hydrogen storage performance of TBAB/SF_6 hydrate solid solution were carried out by the isochoric pressure

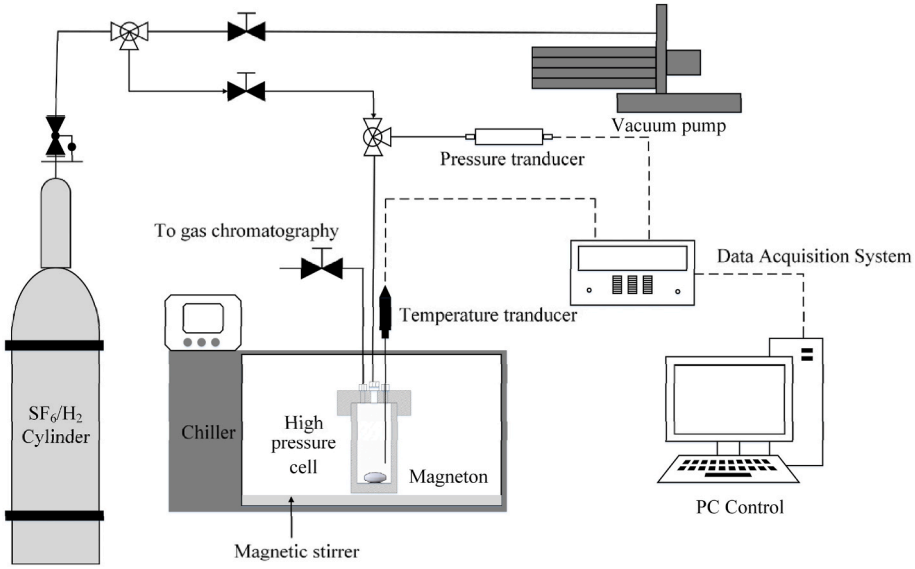

Fig. 1. Schematic of the experimental apparatus.

drop approach. The cell was first cleaned with deionized water and the required solution was loaded into the cell, and the cell was evacuated with a vacuum pump. Then the temperature was regulated to the desired value (298.2 K) and SF_6 and H_2 gas were injected into the cell successively to the required pressure (~21 MPa) with a certain molar ratio of 10 mol%SF_6/90 mol%H_2. After the cell was stable, the stirring was turned on (800 rpm) and the system was cooled to the formation temperature (274.2 K). Hydrate nucleation was identified via simultaneous markers in the temperature and pressure curve - a sudden exothermic spike of the cell temperature or a sudden pressure drop. And the formation process was considered to be completed when the pressure drop was less than 0.01 MPa/h. Then the gas phase component was analyzed by GC.

Raman spectroscopy (Renishaw inVia Basis with an excitation wavelength of 532 nm, a grating of 2400 lines/mm, a laser power of 10 mW and the exposure-time of 10s) was used to analyze the hydrogen molecules occupancy in hydrate cages. A 50X objective allowed for focusing of the incident laser beam and collection of the Raman scattering. The calibration of the spectrometer was done using the 520.7 cm^{-1} mode of a silicon sample. In the case of hydrate measurements, the samples were cooled to 253 K of approximately 7 days to ensure the fully converted state. And then the hydrate samples were ground to the appropriate size under the liquid nitrogen environment. Then the small samples were transferred within 30 s to a temperature-controlled stage (Linkam THMS600), which was set to 173 K to maintain the low-temperature environment required for the measurement. The range of the spectrometer were 4300 cm^{-1}. For each hydrate sample the spectra were confirmed by the results acquired from different locations on the sample. Analysis of the spectra acquired was performed using Renishaw WiRE 3.4 software.

2.3.2. Preparation and characterization for hydrate samples

1) Preparation of the hydrate samples

The apparatus for the preparation of TBAB/SF_6 hydrate solid solution was also shown in Fig. 1. The TBAB solution (~0.30 mol%) was added to the reactor, cooled to 274.15 K and stabilized. Vacuum the reactor with a vacuum pump to ensure that there was no residual air in the cell. Then, the SF_6 was injected into the reactor to preset experimental pressure (~0.85 MPa). After the temperature and pressure of SF_6 inside the reactor stabilized, the magnetic stirring was set up to 800 rpm to accelerate the formation of TBAB/SF_6 hydrate solid solution. Then the reactor was cooled to enough time of approximately 7 days to obtain a sample in a fully converted state. The solid sample was quickly collected and immersed in liquid nitrogen for the subsequent characterization. The preparation procedures for SF_6 hydrates (274.15 K, 0.8 MPa, 600 rpm) and TBAB hydrates (273.15 K, 600 rpm) are similar to the steps described above.

2) Characterization of the hydrate samples

A series of characterization experiments was then conducted to determine the structure properties of the TBAB/SF_6 hydrate solid solution:

Raman spectroscopy: The Raman was also used to analyze TBAB/SF_6 hydrate solid solution, SF_6 hydrates and TBAB hydrates. The experimental procedure is similar to that described above.

PXRD analysis: The PXRD analysis was carried out using X'Pert Pro MPD diffractometer (3Kw, 60 kV,55 mA) which can effectively characterize hydrate samples under low-temperature conditions. TBAB/SF_6 hydrate solid solution, 0.30 mol% TBAB hydrate and SF_6 hydrate samples were quickly transferred to a square test platform using liquid nitrogen. This permits quick and easy recovery of the hydrates while ensuring their stability when exposed to atmospheric pressure. The PXRD patterns were collected with a total 2θ scan time of 1.5 min each, using Cu Kα radiation (λ = 1.5406 Å, 2.2 kW). The 2θ range of 10–55°, step size of 0.01°, and rate of 10° min^{-1} were kept constant throughout.

Differential scanning calorimetry (DSC): DSC experiments were designed to verify the existence of the new structure of TBAB/SF_6 hydrates (TA Instrument, Q20 with the minimum temperature of 93.2 K, a sensitivity of 1 μW, a resolution of 0.04 μW and a dynamic range measurement of ±350 mW). 0.30 mol% TBAB solution or pure water was introduced into the high-pressure crucible (25 μL, ME-30077139) for the formation and dissociation of 0.3 mol%TBAB hydrates, TBAB/SF_6 hydrate solid solution. The sample cell was then pressurized with SF_6 to experimental pressure (~0.85 MPa). The isothermal procedure described in the literature was adopted for all experiments. T was decreased from 293.2 K to 253.2 K at a rate of 0.1 K/min to facilitate 0.3mol% TBAB hydrates, TBAB/SF_6 hydrate solid solution or SF_6 hydrates formation, and then kept at 253.2 K for 4.0 h to ensure complete hydrates formation. Afterward, T was gradually increased to 293.2 K at a rate of 0.05 K/min, in order to melt ice and dissociate hydrate samples.

More details about the PXRD and Raman analysis are available in our previous work [21].

2.4. Data analysis

In this work, the hydrogen storage capacity is the standard gravimetry of hydrogen stored in the gas hydrate phase (wt%) [22].

$$\text{hydrogen storage capacity} = M_{H_2} \cdot \frac{\Delta n}{m_{hydrate}} \times 100\% \quad (1)$$

where M_{H_2} is the molecule mass of hydrogen (2 g/mol); $m_{hydrate}$ is the total mass of the solid hydrate, in this work, it is expressed as the total mass of water, TBAB, and SF_6 in the hydrate phase; Δn is the molar number of hydrogen uptake in hydrates, usually calculated by the equation of state, shown as Eq. (2).

$$\Delta n = n_0 - n_t = \frac{P_0 V_0}{Z_0 R T_0} - \frac{P_t V_t}{Z_t R T_t} \quad (2)$$

where Z is the gas compressibility factor, calculated by the R–K equation in this work; V is the volume of the gas phase in the cell (m^3); R is the universal gas constant (8.314 $J \cdot mol^{-1} \cdot K^{-1}$); P and T are the instantaneous pressure (kPa) and temperature (K) in the cell, respectively.

3. Results and discussion

3.1. Tuning TBAB concentration for preparation of TBAB/SF_6 hydrate solid solution

In the concept of hydrogen storage based on TBAB/SF_6 hydrate solid solution, the primary role of semi-clathrate hydrate was to provide more suitable gas diffusion channels as the significantly low theoretical hydrogen storage capacity of TBAB hydrates (0.362 wt%) compared to the storage capacity of SF_6 hydrates (1.06 wt%). So the concentration of TBAB solution is a key factor. Changes in TBAB concentration can cause a transformation in the configuration of TBAB hydrate [23,24], and TBAB would also compete with SF_6 for water molecules to reduce the storage capacity. So, it is necessary to control the concentration of TBAB to coordinate the balance between diffusion channels and hydrogen storage capacity.

Firstly, the influence of TBAB concentration on the hydrogen storage performance of TBAB/SF_6 mixed hydrate was analyzed. Fig. 2 shows the hydrogen storage capacity of the 10 mol% SF_6/90 mol% H_2 system with TBAB solution at the concentration of 0–2.34 mol% under the conditions of 274.2 K and 21.0 MPa. Compared with the hydrogen storage capacity of the system without TBAB (0.294 wt%), the effect of TBAB concentration on hydrogen storage performance showed the promoting effect firstly, and then turned to the inhibiting effect when the TBAB concentration was around 1.38 mol%. Based on the above results, we can

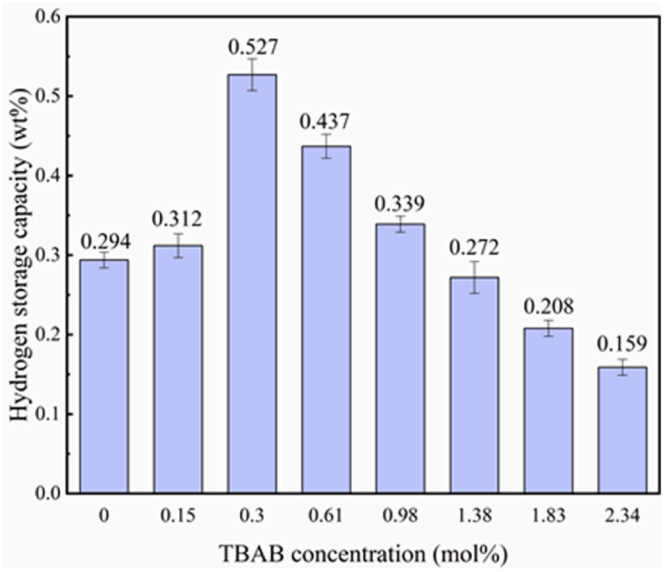

Fig. 2. Effect of TBAB concentration on hydrogen storage performance of TBAB/SF_6 hydrates.

reasonably assume that 0.30 mol%TBAB solution was more likely to form the suitable hydrate solid solution structure with SF_6 to promote hydrogen storage. This was mainly the reason that in our concept, the TBAB hydrate structure was mainly used as the hydrogen diffusion channels to achieve more hydrogen molecules diffuse into the inner hydrate layer, and low-concentration TBAB can do it. However, when TBAB concentration was too low (0.15 mol%), from the perspective of thermodynamic equilibrium [25–27], the structure of SF_6 hydrate would dominate the hydrate phase. And the amount of TBAB hydrates was not significant. In this case, it was difficult to determine whether the low concentration TBAB just transformed into TBAB hydrate or acted the diffusion channel of TBAB/SF_6 hydrate (Supplementary Fig. 1). When TBAB concentrations increased to high concentration, it was easier to form TBAB hydrate, so the redundant TBAB which not participate in the construction of TBAB/SF_6 hydrate solid solution would further compete for water molecules to reduce the hydrogen storage capacity, greatly reduction potential of TBAB/SF_6 hydrate solid solution for hydrogen storage. Based on the above analysis, we believed that low-concentration TBAB (0.30 mol%) would be more conducive to forming the new hydrate solid solution structure with SF_6.

Based on the above analysis, we believed that low-concentration TBAB (0.30 mol%) would be more conducive to forming the new hydrate solid solution structure with SF_6, but had not been confirmed. Actually, the formation of hydrate structures was a process of disordered water molecules to ordinalization, and the key was the conversion of weak hydrogen bonds (~3200 cm^{-1}) to strong hydrogen bonds (~3400 cm^{-1}). Raman spectroscopy can provide related information [28], which is an effective method for analyzing the structures. Fig. 3 shows the Raman spectra of TBAB/SF_6 hydrates formed with different TBAB concentrations, with Raman spectra of pure TBAB hydrate and SF_6 hydrate as blank controls. The peak at ~1110 cm^{-1} can be used as the characteristic peak of TBAB hydrate (Supplementary Fig. 2). As shown in Fig. 3, the structure of TBAB hydrates was formed in different TBAB concentration systems, and the characteristic peak at 769 cm^{-1} attributed to SF_6 in the hydrate cages also indicated the formation of SF_6 hydrate. If TBAB hydrate and SF_6 hydrate only coexist without a new hydrate structure, there would be no new Raman peak. However, a new characteristic peak appeared at 471 cm^{-1} and its intensity was positively correlated with TBAB concentrations. Although it is currently difficult to confirm the explicit assignment of this peak through supplementary experiments or direct literature evidence. Only the TBAB-SF_6 hydrate system shows the peak at 471 cm^{-1}, with a peak position deviation of <1 cm^{-1} in multiple parallel experiments, excluding interference from impurities or instrument noise. The system-specific characteristic of this peak is sufficient to support its use as a marker to distinguish the TBAB/SF_6 hydrate from other systems. And the characteristic peak of SF_6 hydrate was redshifted by 0.7 cm^{-1} [29], suggesting that TBAB and SF_6 formed a more stable hydrate structure, namely TBAB/SF_6 hydrate solid solution.

In addition, the intensity of C–H stretching bands in Fig. 3 appeared inconsistent with TBAB concentrations. In the TBAB concentration range of 0.30–1.38 mol%, the intensity of the C–H stretching peak in the TBAB-SF_6 hydrate system shows a significant positive correlation with TBAB concentration. A significant decrease in the intensity of the C–H stretching peak occurs only when the TBAB concentration reaches 2.34 mol%, which is also consistent with the results of pure TBAB hydrate Raman spectrum (Supplementary Fig. 3). Characteristic peak shifts were observed for the C–H bending vibration peaks (1134 cm^{-1},1445 cm^{-1}, 1451 cm^{-1}) in the low-wavenumber range (Supplementary Fig. 4). This

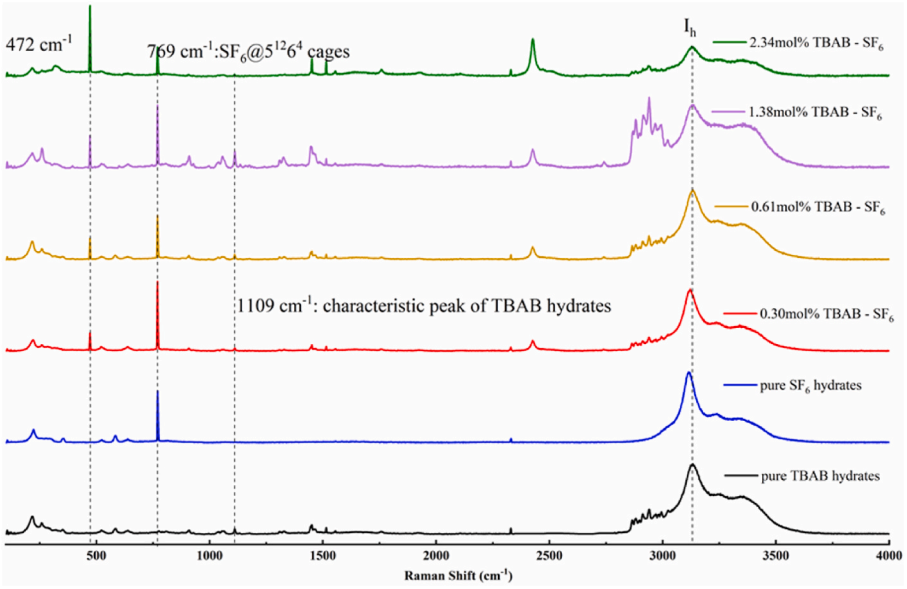

Fig. 3. Raman spectroscopy of TBAB/SF_6 hydrates with different TBAB concentrations.

peak position change is consistent with the literature-reported [30] characteristics of TBAB phase transition. Further comparing the intensity ratio of C–H bonds to ice/hydrate O–H bonds. At 1.38 mol%, the O–H bond signal of TBAB hydrate dominates; while at 2.34 mol%, the O–H bond signal of the ice phase increases significantly, which indicated incomplete TBAB phase transition at this concentration, with residual ice phase structures in some regions—further explaining the rationality of the C–H peak intensity decrease.

The intensity ratio of strong hydrogen bonds to weak hydrogen bonds (I_s/I_w) can effectively reflect the compression/extension of hydrogen bonds to further understand the formation process of TBAB/SF_6 hydrate solid solution [28]. Fig. 4 shows the Raman shifts of strong and weak hydrogen bonds and the corresponding intensity ratios. It can be seen that with the addition of TBAB, a significant red shift (~8 cm^{-1}) in strong hydrogen bonds and a slight blue shift (~2 cm^{-1}) in weak hydrogen bonds. This was mainly the reason that TBAB as an ionic additive, would produce TBA^+ and Br^-. TBA^+ mainly affected strong hydrogen bonds, the strong hydrogen bonds extended and resulting in the improvement in the thermodynamics and kinetics of hydrates. The blue shift of weak hydrogen bonds was influenced by Br^- [31]. The result of weak hydrogen bond compression was that the hydrates were more compact, which was not conducive to providing gas diffusion channels. The ratio (I_s/I_w) showed a rapid increase followed by a decrease as TBAB concentrations changed, and the highest value was obtained at 0.30mol% TBAB solution, indicating the highest degree of water molecule ordering. And the value can be used to semi-quantitatively analyze the hydrogen storage performance of TBAB/SF_6 hydrates, which was consistent with the above experimental results. Based on the comprehensive analysis of the Raman peak shift, new Raman peak, and peak intensity ratio, it could indicate that low-concentration TBAB were more likely to synergistically interact with SF_6 to form a more stable TBAB/SF_6 hydrate solid solution.

3.2. DSC analysis of TBAB/SF_6 hydrate solid solution

The experimental results and Raman analysis both indicated that low-concentration 0.30mol% TBAB form a new hydrate structure with SF_6, exhibiting better hydrogen storage performance. While the new structure would exhibit different phase change temperatures. To further verify the formation TBAB/SF_6 hydrate solid solution, DSC was used to characterize the dissociation temperature of 0.30mol% TBAB + SF_6 hydrate and 2.34 mol% TBAB + SF_6 hydrate. Fig. 5 shows the DSC curves of Ice, 0.30 mol% TBAB hydrate, SF_6 hydrate, and 0.30 mol% TBAB + SF_6 hydrate and 2.34 mol% TBAB + SF_6 hydrate in the temperature range of 268 K–292 K. And the related information is listed in Table 1. It can be seen that the extrapolated onset temperature of the ice phase was 273.26 K, which is close to the melting point of ice (273.15 K), the corresponding melting enthalpy obtained was 328.4 J/g, and the

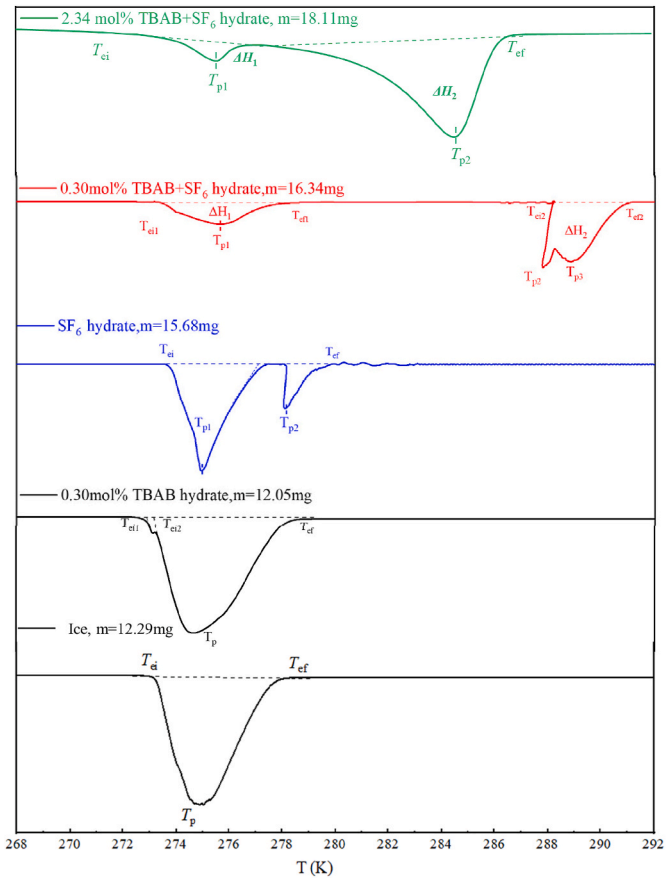

Fig. 5. The DSC measurement curves of ice, 0.30 mol%TBAB hydrates, SF_6 hydrates, 0.30 mol%TBAB + SF_6 mixture hydrates and 2.34 mol%TBAB + SF_6 hydrates.

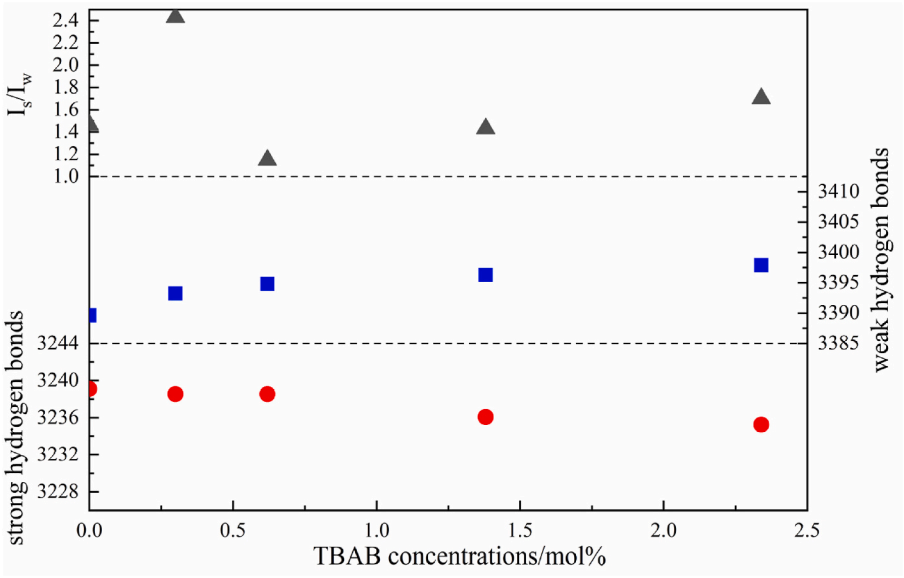

Fig. 4. The Raman position of the peaks corresponding to the strong/weak hydrogen bonds of TBAB/SF_6 hydrates with different TBAB concentrations.

Table 1
The temperature and enthalpy of different systems obtained in DSC experiments[a].

System	T_{ei}/K	T_p/K	T_{ef}/K
Ice	273.26	275.33	277.39
0.30mol%TBAB hydrate	273.05	274.68	277.81
	273.19		
SF_6 hydrate	273.81	274.98	276.81
		278.08	
0.30mol%TBAB + SF_6 hydrate	273.32	274.98	276.81
	288.21	287.78	290.63
		288.84	
2.34 mol%TBAB + SF_6 hydrate	274.08	275.5	286.00
		284.45	

[a] T_{ei} and T_{ef} are the extrapolated onset temperature and extrapolated end temperatures, respectively; T_p is the peak temperature.

standard melting enthalpy of ice is 335 J/g [32], with a deviation of only 1.97 %. It can be also found that the peak width of 0.30 mol% TBAB hydrate corresponding to the ice phase was extended, and the peak shape was also significantly changed. The melting point of the ice phase decreased to 273.05 K [33], and a stepped peak appeared near the ice peak, similar to the glass transition temperature, It may represent the process of amorphous phase growing into the hydrate crystalline phase in the solution, which was only observed in low-concentration TBAB hydrate systems. For SF_6 hydrate, the extrapolated onset temperature of ice phase (273.81K) shifted to the right by about 0.6 K, but the peak shape of the ice phase did not change significantly and basically overlapped; The temperature peak appearing at ~278K indicated SF_6 hydrate.

In the DSC curve of 0.30 mol% TBAB + SF_6 hydrate, there was no significant change of the ice phase, and no peak attributed to SF_6 hydrate was found near 278 K. However, in the high-temperature range (288 K–291K), an obvious set of overlapping peaks was discovered, mainly including two distinct peaks with temperatures of 287.78 K and 288.84 K, respectively. Firstly, a second-order polynomial was used to fit the phase equilibrium data of SF_6 hydrate [34], the corresponding pressure was calculated to be 1.63 MPa. And SF_6 would already be liquefied under this condition, so the possibility of SF_6 hydrate was ruled out. While in the DSC curve of 2.34 mol% TBAB + SF_6 hydrate, two distinct peaks disappeared and the characteristic peak of TBAB hydrates only appears at the temperature of 284.45 K. At higher TBAB concentrations, TBAB hydrates were formed preferentially. After the gas–liquid interface was covered with the TBAB hydrate film, the diffusion channel of gas guest molecules was hindered, and the formation of SF_6 hydrate structures was also prevented. Therefore, compared with the DSC curve of 0.30 mol% TBAB + SF_6 hydrate, SF_6 hydrate was unstable with 2.34 mol % TBAB solution, but TBAB hydrate could form more completely. Based on the above discussion and related study support [35], the peak temperature at 288.84 K of 0.30 mol% TBAB + SF_6 hydrate system was attributed to a new hydrogen bond network, TBAB/SF_6 hydrate solid solution, formed by the low-concentration 0.30 mol% TBAB hydrate and SF_6 hydrate by the common building blocks, which exhibited a more stable thermodynamic performance. And the peak at 287.78 K was attributed to high-concentration TBAB hydrates, because most of the host water molecules may be consumed by the formation of TBAB/SF_6 hydrate solid solution, and the residual water for the crystallization of TBAB hydrate may face a water shortage in 0.30 mol% TBAB solution, so the peak attributed to TBAB hydrates was shifted towards the high-temperature area compared to the 0.30 mol% TBAB hydrate.

3.3. PXRD analysis of TBAB/SF_6 hydrate solid solution

The structure of TBAB/SF_6 hydrate solid solution was further confirmed by PXRD (see Fig. 6). * represents the hexagonal ice peaks. Characteristic peaks of 0.30 mol% TBAB + SF_6 hydrate at 21.08°, 29.80°, and 31.18° were observed, corresponding to the Miller indices of (4 0 0), (4 4 0), and (5 3 1) of type-sII hydrate structure [36], respectively. And it could be seen that the amount of TBAB hydrates was not significant, some characteristic peaks attributed to TBAB hydrate have disappeared, but the characteristic peaks at 16.4° and 33.8° that different from those of sII hydrates structure were observed, and the peaks were assigned to the structure of TBAB hydrate [37], which still proving the existence of TBAB hydrate structure. The main composition of the TBAB/SF_6 hydrate solid solution was sII hydrate structure. The low concentrations of TBAB formed a small proportion of TBAB hydrate, and TBAB hydrate was just served as the hydrogen diffusion channel which connected to the main sII hydrate structure by the common building blocks. So the characteristic peaks attributed to TBAB hydrate at the boundary of SF_6 hydrate and TBAB hydrate lose their response.

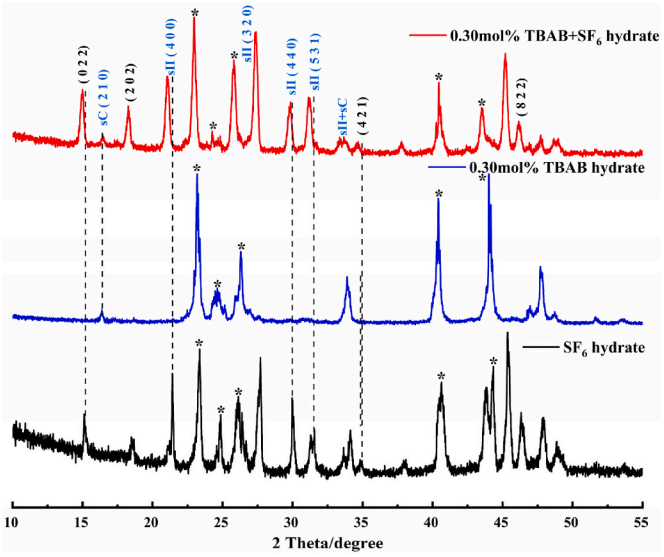

Fig. 6. PXRD patterns of the 0.30 mol% TBAB + SF_6 hydrate, 030 mol% TBAB hydrate and SF_6 hydrate * represents hexagonal ice peaks.

The distribution pattern of characteristic peaks in PXRD is determined by the size, shape, and orientation of the unit cell. Compared with the patterns of SF_6 hydrate and 0.30 mol% TBAB hydrate, the characteristic peaks of 0.30 mol% TBAB + SF_6 hydrate sample, which belongs to SF_6 hydrate and TBAB hydrate, showed significant shifts. The characteristic peaks of SF_6 hydrate were shifted to the left by an average of 0.3°, while those belonging to TBAB hydrate were shifted to the right by 0.1°. The overall shift of these characteristic peaks reflected the changes in unit cell parameters and crystal distortion. The leftward shift of the characteristic peak of SF_6 hydrate indicated an increase in unit cell parameters and a decrease in interplanar spacing, while the corresponding unit cell constant of TBAB hydrate decreased. It should be particularly noted that if TBAB hydrate and SF_6 hydrate were simply physically mixed (without structural interaction), the characteristic peaks of the two components would remain at their original positions, with only peak intensities superimposed in proportion. However, the systematic shift of characteristic peaks in this study (left shift of SF_6 peaks and right shift of TBAB peaks) proves that the crystal structures of the two hydrates have undergone reconstruction due to interaction, rather than simple coexistence. This is essentially different from the diffraction characteristics of "physical mixing" and is a direct signal for the formation of a new solid solution structure.

Chen et al. [38] revealed that there were inherent relations in different hydrate crystal structures. The host water molecules can generate different hydrogen bond network structures through the common building blocks. In this study, since the Br–O bond length in TBAB is longer than the O–O bond length between water molecules [39], TBAB hydrate exerts an outward tensile force on the adjacent SF_6

hydrate clathrates, leading to the expansion of the SF_6 clathrate unit cell (peak left shift); at the same time, the reaction force of the SF_6 clathrates compresses the TBAB clathrates, causing the contraction of the TBAB clathrate unit cell (peak right shift). Finally, an "interacting clathrate network" (solid solution structure) is formed. The "loose TBAB hydrate + expanded SF_6 hydrate" combination formed by this structural reconstruction provides an exclusive channel for hydrogen molecule transport and storage. H_2 molecules can penetrate the loose TBAB clathrates, enter the expanded SF_6 hydrate cages, and stably occupy them. So the hydrogen storage performance highly depended on the unique structure of TBAB/SF_6 hydrate solid solution.

3.4. Hydrogen storage performance of TBAB/SF_6 hydrate solid solution

Raman, DSC, and XRD analysis all indicated that the formation of the new structure of TBAB/SF_6 hydrate solid solution at the specific 0.30 mol% TBAB concentration, and the enclathrated amount of SF_6 could reach 56.25 mmol, which could be converted to 63 vol stored at standard atmospheric pressure per volume of hydrate (Supplementary Fig. 5). Meanwhile, the hydrogen storage performance could further support the exist of this structure and understand the potential application in energy storage. In our recent study [40], we have determined the hydrate phase equilibrium data of the 10mol% SF_6/90mol% H_2+0.3 mol% TBAB solution system, and the results (Supplementary Fig. 6) showed the combination of TBAB and SF_6 could further mild the formation conditions compared to the literature data [25,27]. Further analysis showed that hydrogen molecules were not simply occupying the small cages of SF_6 hydrates and TBAB hydrates, respectively, a more stable hydrate structure was formed, which hydrogen molecules can be stored stably in this structure under milder conditions. The phase equilibrium data to some extent further confirmed the formation of TBAB/SF_6 hydrate solid solution, and the excellent thermodynamic stability of TBAB/SF_6 hydrate solid solution was also indicated.

Subsequently, further analysis of the hydrogen storage performance of TBAB/SF_6 hydrate solid solution was conducted. Fig. 7 shows the temperature and pressure evolution corresponding to the hydrogen storage process of TBAB/SF_6 hydrate solid solution and the control group of SF_6. The characteristic phenomena of pressure drop and temperature rise indicated the formation of hydrates. And the pressure drop of TBAB/SF_6 hydrate solid solution system was about 1.2 MPa, with a relatively high-temperature rise of about 5 K, indicating a more intense hydration reaction compared with the control group.

The hydrogen storage capacity was calculated based on temperature and pressure changes, and the results were shown in Fig. 8. Compared

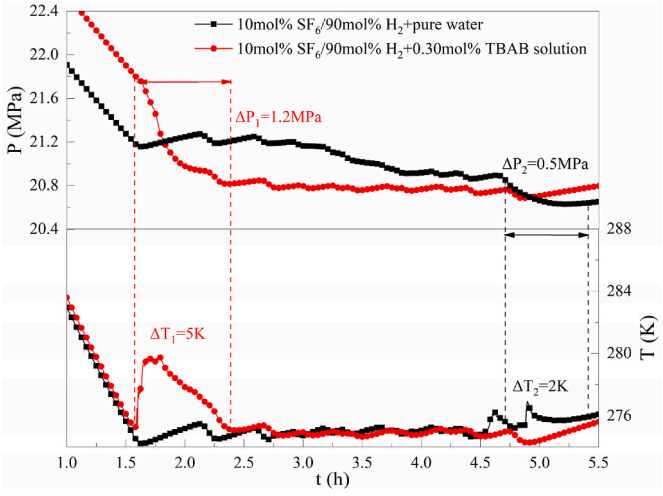

Fig. 7. Evolution of pressure and temperature during H_2 in TBAB/SF_6 hydrate solid solution.

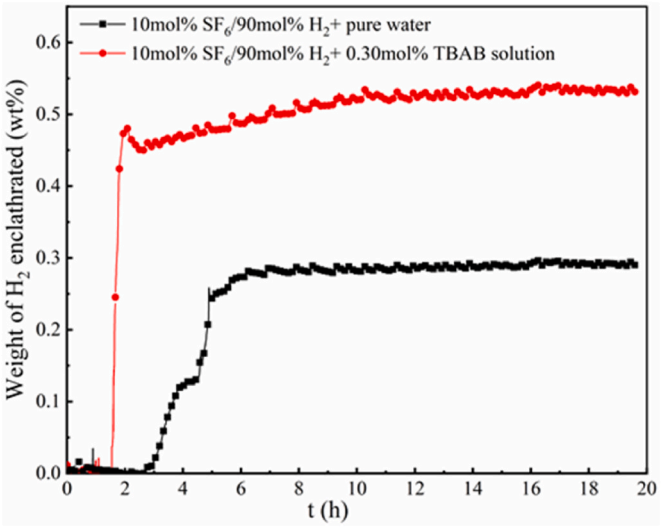

Fig. 8. Effect of TBAB/SF_6 hydrate solid solution on hydrogen storage capacity (C_{TBAB} = 0.3 mol%, P = 21 MPa, T = 274.2 K).

with the pure SF_6+H_2 or 0.30mol% TBAB + H_2 systems, the system of TBAB/SF_6 hydrate solid solution for hydrogen storage exhibited completely different formation kinetics, with the characteristics of a two-step growth process. The first stage was the rapid hydrogen storage stage, where a high hydrogen storage capacity of 0.590 wt% within 30 min was achieved, and ultra-rapid hydrate growth in a short time. This phenomenon had similar growth kinetics characteristics to our previous study of propane as the thermodynamic additive [41], by adjusting the propane and hydrogen distribution at the gas-liquid interface to achieve the transformation of hydrate nucleation mode, breaking through the limitation of the number of hydrate crystal nuclei in the hydrate growth process and achieving rapid hydrogen storage. However, compared with the hydrogen storage capacity of the propane + H_2+water system (0.256 wt%) [41] and the SF_6+H_2+water system (0.294 wt%) in this study, the addition of 0.30mol% TBAB to the SF_6+H_2+water system has achieved a significant breakthrough in hydrogen storage capacity, mainly due to the milder formation conditions for the greater driving force, the conversion of water-to-hydrate was increased. Meanwhile, the low-concentration TBAB could avoid low storage capacity caused by the high-concentration TBAB, as the overfitting between cations of TBAB and the hydrate cages to reduce the storage capacity.

The second stage was the slow hydrogen storage stage, where the hydrogen molecules diffusion into the hydrate layer at a relatively constant rate for about 8 h, and the hydrogen storage capacity increased from 0.453 wt% to 0.527 wt% (Supplementary Fig. 7). The stage was quite different from our previous study [41] and the control groups, the hydrogen storage capacity of those systems remained almost stable after the rapid growth stage. The main reason for the difference was that during the subsequent hydrate growth process, the regular 5^{12} cages formed a well-ordered barrier to hinder the diffusion of hydrogen molecules into the inner hydrate layer, so the hydrate growth rate was severely restricted by the hydrogen diffusion rate, while the main structure of TBAB/SF_6 hydrate solid solution was sII SF_6 hydrates, served as the storage site, so no significant changes in the theoretical storage capacity of TBAB/SF_6 hydrate solid solution. While the relatively loose TBAB hydrates were connected to provide hydrogen diffusion channels through the common building block (5^{12} cages). So compared to sII hydrates, TBAB/SF_6 hydrate solid solution had certain lattice defects, allowing more hydrogen molecules to diffuse into the inner hydrate cages and the number of effective hydrate cages for hydrogen was significantly increased. Based on the above characteristics, the process of hydrogen storage based on TBAB/SF_6 hydrate solid solution can be divided into two stages: the first stage was controlled by

the thermodynamic and nucleation mode, the rapid hydrate growth process was realized by the milder phase equilibrium conditions and the transition of hydrate nucleation mode; The second stage was controlled by the hydrogen diffusion, the bulk diffusion of hydrogen into the inner hydrate cages was enhanced by the more favorable mass transfer channels provided by TBAB hydrates, effectively improving the conversion rate of water-to-hydrate. The concept of TBAB/SF[6] hydrate solid solutions provides a new approach and solution for hydrate-based hydrogen storage technology with better gas storage capacity.

3.5. Hydrogen occupaancy behavior in TBAB/SF_6 hydrate solid solution

The above results have shown the excellent performance of TBAB/SF_6 hydrate solid solution in hydrogen storage. And the occupancy behavior of hydrogen molecules would advance the practical applications and further developments of this structure. Fig. 9 shows the Raman spectra in the range of 4000~4300 cm^{-1} for H_2 in TBAB/SF_6 hydrate solid solution. The Raman peaks of all samples around 4127 cm^{-1} was attributed to single hydrogen molecule in the small cages ($1H_2@5^{12}$ cage). A characteristic peak (~4156 cm^{-1}) indicating the hydrogen occupancy behavior was also observed with 0.3 mol% and 0.61 mol% TBAB solution. The features of characteristic peaks become more obvious and an additional peak (4163 cm^{-1}) was observed only with 0.3 mol% TBAB solution, validating that SF_6 and TBAB can form TBAB/SF_6 hydrate solid solution only at low TBAB concentration, and this looser structure could allow multiple hydrogen molecules to be loaded in the cages for higher storage capacity.

The study [42] showed that the vibration peak of H_2 gas phase was around 4155 cm^{-1}. And related study has found the Raman shifts corresponding to hydrogen molecules in the large cages were all lower than 4155 cm^{-1} [43]. Therefore, the two Raman characteristic peaks above 4155 cm^{-1} did not belong to the hydrogen molecules in the large cages. So the three Raman characteristic peaks at 4127.6, 4156, and 4163 cm^{-1} were all tentatively assumed to hydrogen molecules in the small cages of TBAB/SF_6 hydrate solid solution. The Raman peak around 4127 cm^{-1} was attributed to single hydrogen molecule in the small cages ($1H_2@5^{12}$cage) [44]. The theoretical calculation [45,46] indicated that the Raman peaks of double hydrogen molecules in the small cage ($2H_2@5^{12}$ cage) were expected to be above 4155 cm^{-1}. So the two characteristic peaks at 4156 and 4163 cm^{-1} were assigned to $2H_2@5^{12}$ cage of TBAB/SF_6 hydrate solid solution. The blue shift behavior of the two peaks to the high-frequency side compared to the gas phase indicated $2H_2@5^{12}$ cage in the confined space was unstable [21]. And $2H_2@5^{12}$ cage of TBAB/SF_6 hydrate solid solution also exhibited different hydrogen occupancy behaviors. TBAB/SF_6 hydrate solid solution was generated via assembly of the common building block (5^{12} cages) of type-sII SF_6 hydrate and TBAB semi-clathrate hydrate, which contain the two different 5^{12} cages provided by SF_6 hydrate and TBAB hydrate. The small cages of SF_6 hydrate served as the main site of TBAB/SF_6 hydrate solid solution for hydrogen storage. And further analysis of the integrated area of the two characteristic peaks, so it can be concluded that the characteristic peaks at 4156 and 4163 cm^{-1} respectively belong to double H_2 occupation in sII 5^{12} cages and semi-clathrate 5^{12} cages of TBAB/SF_6 hydrate solid solution.

The stability of hydrogen molecules in TBAB/SF_6 hydrate solid solution was explored further. Fig. 10 showed the cumulative decomposition curves (4000~4300 cm^{-1}) of hydrogen molecules in TBAB/SF_6 hydrate solid solution at different TBAB concentrations. It could be seen that from the decomposition curve, it can be observed that the characteristic peak of $1H_2@5^{12}$cage (4127.6 cm^{-1}) is basically stable during the decomposition process when the TBAB concentration is 0.30 mol%. However, considerable declines in the intensity of the two other Raman peaks (4156 and 4163 cm^{-1}) of $2H_2@5^{12}$ cage were observed after 12 min, which was caused by the rupture of the hydrate cages. The reason for the difference between the decomposition behavior was that the free energy of $2H_2@5^{12}$ cage was relatively high and the stability was poor. The hydrate structure is more likely to collapse with the escape of hydrogen molecules. Meanwhile, the intensity of the peak corresponding to $1H_2@5^{12}$cage did not show a paradoxical increase after the decomposition of $2H_2@5^{12}$ cage, indicating that the escape of hydrogen molecules from cages was complete, which ruled out the possibility of hydrogen escaped from $2H_2@5^{12}$ cage to form involve $1H_2@5^{12}$ cgae.

Based on the hidden symmetries contained in clathrate hydrates crystals and intrinsic relations among them given by Chen et al. and experimental results of Raman, DSC and PXRD in this work, a reasonable speculation of the schematic illustration of the mechanisms of TBAB/SF_6 hydrate solid solution was given in Fig. 11. The hydrogen bonding network of clathrate hydrate had its intrinsic relations, which different hydrate structures could be formed by the assembly of common building blocks [38]. So in this work, a new hydrogen bonding network, namely TBAB/SF_6 hydrate solid solution, was constructed by the common 5^{12} cages of low-concentration TBAB hydrate and SF_6 hydrate. The systematic shift of characteristic peaks in PXRD and Raman spectrum of this study proves that the crystal structures of the two hydrates have

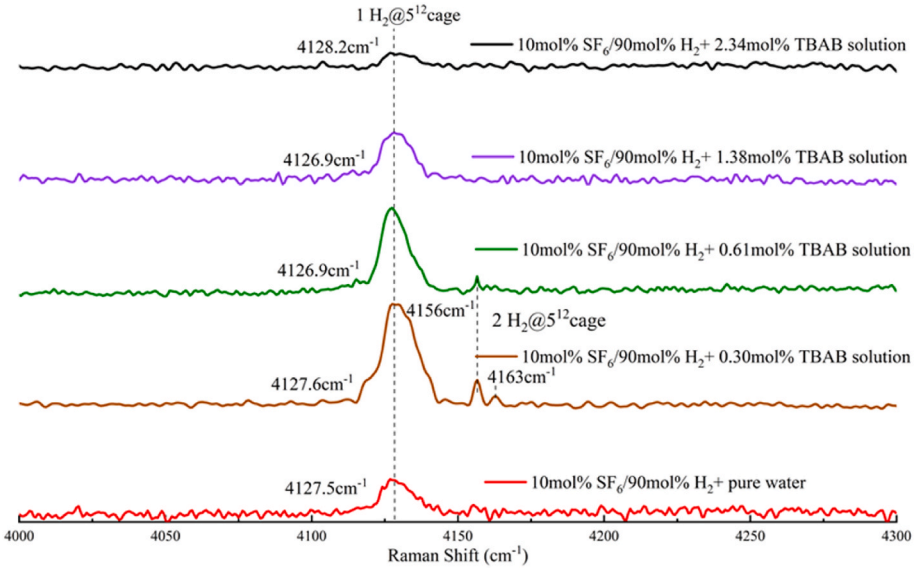

Fig. 9. Raman spectra of the H–H region for H_2 in TBAB/SF_6 hydrate solid solution.

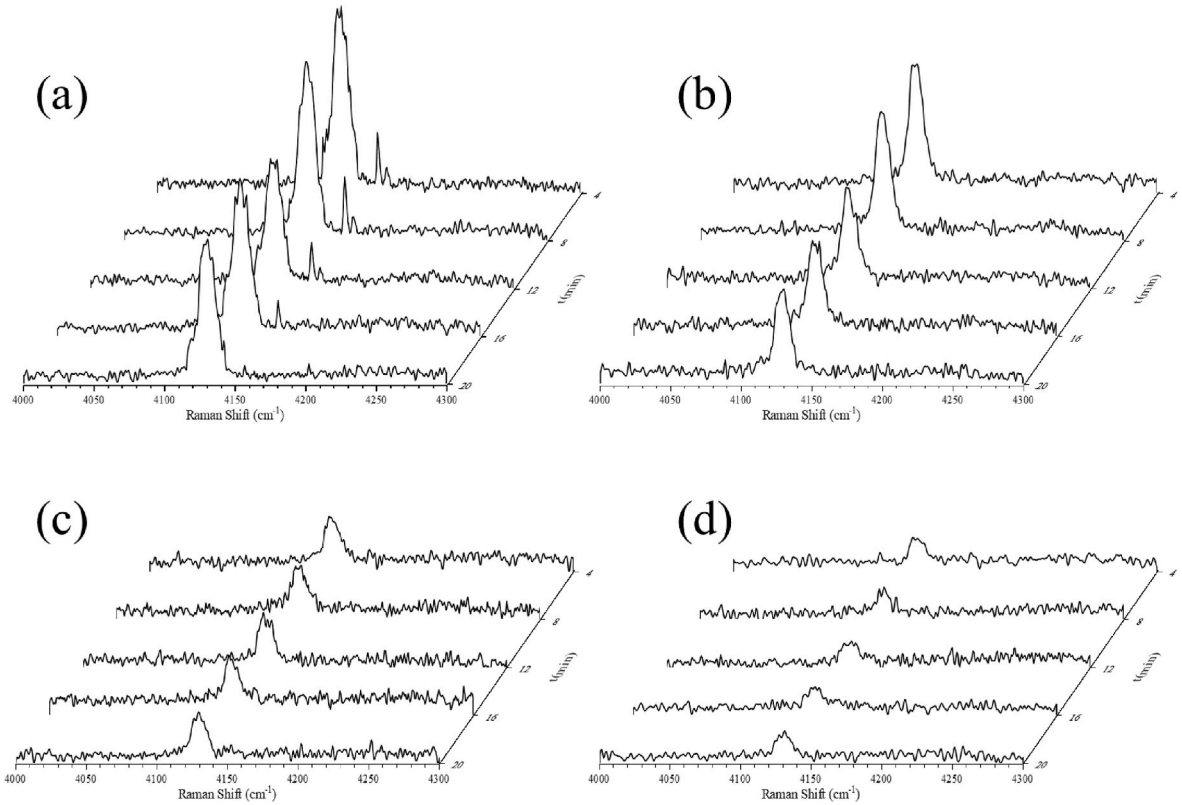

Fig. 10. Raman spectroscopy of the decomposition of H_2 in TBAB/SF_6 hydrate solid solution (a) 0.30mol% TBAB, (b) 0.61 mol% TBAB, (c) 1.38mol% TBAB and(d) 2.34mol% TBAB.

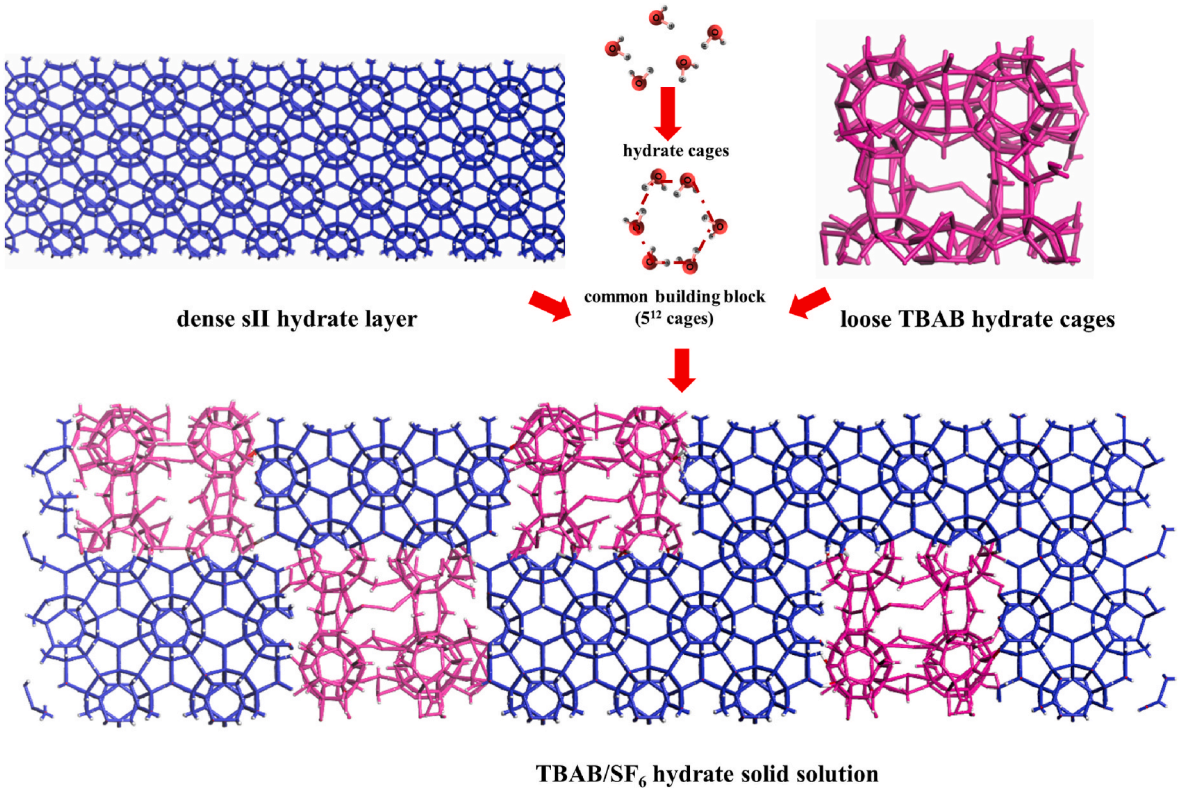

Fig. 11. Schematic illustration of the mechanisms of TBAB/SF_6 hydrate solid solution.

undergone reconstruction due to interaction, rather than simple coexistence. TBAB/SF_6 hydrate solid solution would cause lattice defects

of type-sII SF_6 hydrates, which were regarded as the main sites for hydrogen storage. And the relatively loose TBAB hydrate cages provided the hydrogen diffusion channels for more effective hydrate cages. The cages of TBAB/SF_6 hydrate solid solution exhibited greater deformation while maintaining its regular cage structure, making it easier for hydrogen to diffuse and occupy the hydrate cages. The hydrogen storage performance also depends on the unique structure of TBAB/SF_6 hydrate solid solution, thereby a further increase in the potential of TBAB/SF_6 hydrate solid solution as the hydrogen storage material. However, the specific hydrogen bond connection sites of TBAB/SF_6 hydrate solid solution in Fig. 11 were not clear, which could be further verified by simulating the cage assembly path of TBAB and SF_6 molecules during hydrate formation with MD in future research.

4. Conclusions

We reported a new hydrate crystalline hydrogen bond network, TBAB/SF_6 hydrate solid solution, which was formed by SF_6 hydrate and TBAB hydrate through the common building blocks (5^{12} cages). Based on TBAB/SF_6 hydrate solid solution, we verified the structure and futher revealed the intrinsic relationship between the structure and hydrogen storage performance, some interesting conclusions can be drawn.

(1) TBAB showed the promoting effect firstly, and then turned to the inhibiting effect when the TBAB concentration was around 1.38 mol%. And low-concentration 0.30 mol%TBAB was more likely to form the suitable hydrate solid solution structure with SF_6. The characterizations further verified the formation of the new structure of TBAB/SF_6 hydrate solid solution.
(2) TBAB/SF_6 hydrate solid solution showed excellent thermodynamic stability, the peak temperature at 288.84 K of DSC curve was attributed to the TBAB/SF_6 hydrate solid solution structure, and the equilibrium temperature was shifted up to a higher temperature region under the same pressure.
(3) The structure also exhibited outstanding hydrogen storage performance with the characteristics of two-step hydrate growth. The characteristic peaks shift of PXRD indicated the lattice distortion, with more loose 5^{12} cages for hydrogen diffusion into the inner hydrate layer. So the second slow hydrogen storage stage was strengthened, where the storage capacity increased from 0.453 wt% to 0.527 wt% at a relatively constant rate for about 8 h. And the bulk diffusion of hydrogen into the inner hydrate cages was enhanced by the more favorable mass transfer channels provided by TBAB hydrates, effectively improving the conversion rate of water-to-hydrate. Raman analysis further indicated the phenomenon of double hydrogen molecules occupancy in the small cages of TBAB/SF_6 hydrate solid solution, the characteristic peaks at 4156 cm^{-1} and 4163 cm^{-1} were attributed to $2H_2@5^{12}$ cage in sII 5^{12} cages and semi-clathrate 5^{12} cages of TBAB/SF_6 hydrate solid solution, respectively.

The new TBAB/SF_6 hydrate solid solution structure provides more effective hydrate cages for hydrogen store, with faster formation rate and higher hydrogen storage capacity. This work shows a new idea for hydrate-based hydrogen storage technology.

CRediT authorship contribution statement

Siyuan Chen: Writing – original draft, Formal analysis. **Xinying Li:** Methodology. **Yanhong Wang:** Writing – review & editing, Supervision, Project administration, Conceptualization. **Shuanshi Fan:** Formal analysis. **Xuemei Lang:** Data curation. **Hongfeng Lu:** Formal analysis. **Gang Li:** Validation.

Declaration of competing interest

The authors declare that they have no known competing financial interests or personal relationships that could have appeared to influence the work reported in this paper.

Acknowledgements

This work was supported by the Key Research & Development Program of Guangzhou (No.202206050002).

Appendix A. Supplementary data

Supplementary data to this article can be found online at https://doi.org/10.1016/j.ijhydene.2025.153331.

Data availability

The essential data supporting the major conclusions of this study are present in the paper. Requests for additional information related to the study can be directed to the authors.

References

[1] Momirlan M, Veziroglu TN. Current status of hydrogen energy. Renew Sustain Energy Rev 2002;6:141–79.
[2] MsaND Sankir. Hydrogen storage technologies. Scrivener Publishing LLC; 2018.
[3] Chen Z, Kirlikovali KO, Idrees KB, Wasson MC, Farha OK. Porous materials for hydrogen storage. Chem 2022;8:693–716.
[4] Ulucan TH, Akhade SA, Ambalakatte A, Autrey T, Cairns A, Chen P, et al. Hydrogen storage in liquid hydrogen carriers: recent activities and new trends. Prog Energy 2023;5:012004.
[5] Lang XM, Zheng CJ, Fan SS, Wang YH, Li G, Wang SL, et al. "Similar self-preservation" and decomposition kinetics of tetrahydrofuran-hydrogen hydrate particles. Int J Hydrogen Energy 2022;47:8457–66.
[6] Gupta A, Baron GV, Perreault P, Lenaerts S, Ciocarlan R-G, Cool P, et al. Hydrogen clathrates: next generation hydrogen storage materials. Energy Storage Mater 2021;41:69–107.
[7] Sloan ED, Carolyn K. In: Clathrate hydrates of natural gases. thrid edition ed 2007.
[8] Mao Mao H k WL. Hydrogen storage in molecular compounds. Proc Natl Acad Sci 2004;101(3):708–10.
[9] Mao WL. Hydrogen clusters in clathrate hydrate. Science 2002;297:2247–9.
[10] Florusse LJ, Peters CJ, Schoonman Joop, Hester Keith C, Koh Carolyn A, Dec Steven F, et al. Stable low-pressure hydrogen clusters stored in a binary clathrate hydrate. Science 2004;306:469–71.
[11] Veluswamy HP, Kumar R, Linga P. Hydrogen storage in clathrate hydrates: current state of the art and future directions. Appl Energy 2014;122:112–32.
[12] Zhang JB, Li Y, Yin ZY, et al. Coupling amino acid L-Val with THF for superior hydrogen hydrate kinetics: implication for hydrate-based hydrogen storage. Chem Eng J 2023;467:143459.
[13] Kim K, Lee W, Lee J, Lee JW. Water-in-oil emulsions as micro-reactors for achieving extremely rapid and high hydrogen uptakes into clathrate hydrates. Chem Eng J 2024;499:156666.
[14] Kong Y, Yu H, Liu M, Zhang G, Wang F. Ultra-rapid formation of mixed H_2/DIOX/THF hydrate under low driving force: important insight for hydrate-based hydrogen storage. Appl Energy 2024;362:123029.
[15] Kim M-K, Ahn Y-H. Gas hydrates for hydrogen storage: a comprehensive review and future prospects. Korean J Chem Eng 2024;41:73–94.
[16] Wang Y, Yin K, Lang X, Fan SS, Li G, Yu C, et al. Hydrogen storage in sH binary hydrate: insights from molecular dynamics simulation. Int J Hydrogen Energy 2021;46:15748–60.
[17] Wang YH, Yin KD, Fan SS, Lang XM, Yu C, Wang SL, et al. The molecular insight into the "Zeolite-ice" as hydrogen storage material. Energy 2021;217:119406.
[18] Hasegawa T, Brumby PE, Yasuoka K, Sum AK. Mechanism for H_2 diffusion in sII hydrates by molecular dynamics simulations. J Chem Phys 2020;153:054706.
[19] Gorman PD, English NJ, Macelroy JMD. Dynamical cage behaviour and hydrogen migration in hydrogen and hydrogen-tetrahydrofuran clathrate hydrates. J Chem Phys 2012;136:1–7.
[20] Shimada W, Shiro M, Kondo H, Takeya S, Oyama H, Ebinuma T, et al. Tetra-n-butylammonium bromide–water (1/38). Acta Crystallogr Sect C:Cryst Struct Commun 2005;61:o65–6.
[21] Chen S, Wang Y, Fan S, Lang X, Li G. Intriguing phenomenon of hydrogen molecules occupancy in clathrate hydrate cages: implications for hydrogen storage. Chem Eng J 2024;499:156089.
[22] Chen SY, Wang YH, Lang XM, Fan S, Li G. Rapid and high hydrogen storage in epoxycyclopentane hydrate at moderate pressure. Energy 2023;268:126638.
[23] Oyama H, Shimada W, Ebinuma T, Kamata Y, Takeya S, Uchida T, et al. Phase diagram, latent heat, and specific heat of TBAB semiclathrate hydrate crystals. Fluid Phase Equilib 2005;234:131–5.

[24] Aladko LS, Dyadin YA, Rodionova TV, Terekhova IS. Effect of size and shape of cations and anions on clathrate formation in the system: halogenides of quaterly ammonium bases and water. J Mol Liq 2003;106:229–38.
[25] Park D-H, Lee BR, Sa J-H, Lee K-H. Gas hydrate phase equilibrium for mixtures of sulfur hexafluoride and hydrogen. J Chem Eng Data 2012;57:1433–6.
[26] Hashimoto S, Murayama S, Sugahara T, Sato H, Ohgaki K. Thermodynamic and Raman spectroscopic studies on H_2 + tetrahydrofuran +water and H_2+ tetra-n-butyl ammonium bromide +water mixtures containing gas hydrates. Chem Eng Sci 2006;61:7884–8.
[27] Mohammadi AH, Eslamimanesh A, Belandria V, Richon D. Phase equilibria of semiclathrate hydrates of CO_2, N_2, CH_4, or H_2 + tetra-n-butylammonium bromide aqueous solution. J Chem Eng Data 2011;56:3855–65.
[28] Zhang W, Xu C-G, Li X-S, Huang Z-Y, Chen Z-Y. Microscopic study on the key process and influence of efficient synthesis of natural gas hydrate by in situ Raman analysis of water microstructure in different systems with temperature drop. J Energy Chem 2023;82:317–33.
[29] Lee BR, Lee JD, Lee HJ, Ryu YB, Lee MS, Kim YS, et al. Surfactant effects on SF_6 hydrate formation. J Colloid Interface Sci 2009;331:55–9.
[30] Oshima M, Kida M, Nagao J. Hydration numbers and thermal properties of tetra-n-butyl ammonium bromide semiclathrate hydrates determined by ion chromatography and differential scanning calorimetry. J Chem Thermodyn 2018; 123:32–7.
[31] Raymond EA, Richmond GL. Probing the molecular structure and bonding of the surface of aqueous salt solutions. J Phys Chem B 2004;108:5051–9.
[32] Li G, Liu D, Xie Y. Study on thermal properties of TBAB–THF hydrate mixture for cold storage by DSC. J Therm Anal Calorim 2010;102:819–26.
[33] Massoudi R, King Jr AD. Effect of pressure on the surface tension of aqueous solutions. Adsorption of hydrocarbon gases, carbon dioxide, and nitrous oxide on aqueous solutions of sodium chloride and tetrabutylammonium bromide at 25.deg. J Phys Chem 1975;79:1670–5.
[34] Sugahara K, Yoshida M, Sugahara T, Ohgaki K. Thermodynamic and Raman spectroscopic studies on pressure-induced structural transition of SF_6 hydrate. J Chem Eng Data 2006;51:301–4.
[35] Mahmoudi B, Naeiji P, Varaminian F. Study of tetra-n-butylammonium bromide and tetrahydrofuran hydrate formation kinetics as a cold storage material for air conditioning system. J Mol Liq 2016;214:96–100.
[36] Zang X, Li H, Zhang Y, Chen Y, He Y, Wu N, et al. Experimental investigation on the synergistic influence of tetra-n-butyl ammonium bromide(TBAB) and cyclopentane (CP) in hydrate-based gas separation. Sep Purif Technol 2023;320:124064.
[37] Zhou X, Long Z, He Y, Shen X, Liang D. Phase equilibria and the crystallographic properties of TBAB–CO_2 semiclathrate hydrates. J Chem Eng Data 2018;63: 1249–55.
[38] Chen Y, Takeya S, Sum AK. Topological dual and extended relations between networks of clathrate hydrates and Frank-Kasper phases. Nat Commun 2023;14: 596.
[39] Shimada W, Ebinuma T, Oyama H, Kamata Y, Narita H. Free-growth forms and growth kinetics of tetra-n-butyl ammonium bromide semi-clathrate hydrate crystals. J Cryst Growth 2005;274:246–50.
[40] Wang Y, Chen S, Li X, Lang X, Li G, Fan S. Hydrate phase equilibrium of hydrogen with THP, DCM, TBAB+THF and sulfur hexafluoride +TBAB aqueous solution systems. Fluid Phase Equilib 2025;590:114282.
[41] Chen S, Wang Y, Fan S, Lang XM, Li G. An innovative nucleation method for high and rapid hydrogen storage based on clathrate hydrates. J Mater Chem A 2024: 11424–38.
[42] Trueba AT, Radović IR, Zevenbergen JF, Kroon MC, Peters CJ. Kinetics measurements and in situ Raman spectroscopy of formation of hydrogen–tetrabutylammonium bromide semi-hydrates. Int J Hydrogen Energy 2012;37:5790–7.
[43] Lu QN, He X, Hu WX, Chen XJ, Liu JF. Stability, vibrations, and diffusion of hydrogen gas in clathrate hydrates: insights from Ab initio calculations on condensed-phase crystalline structures. J Phys Chem C 2019;123:12052–61.
[44] Zaghloul MAS, Celli M, Salem NM, Elsheikh SM, Ulivi L. High pressure synthesis and in situ Raman spectroscopy of H_2 and HD clathrate hydrates. J Chem Phys 2012;137:164320.
[45] Wang J, Lu H, Ripmeester JA. Raman spectroscopy and cage occupancy of hydrogen clathrate hydrate from first-principle calculations. J Am Chem Soc 2009; 131:14132–3.
[46] Wang J, Lu H, Ripmeester JA, Becker U. Molecular-dynamics and first-principles calculations of Raman spectra and molecular and electronic structure of hydrogen clusters in hydrogen clathrate hydrate. J Phys Chem C 2010;114:21042–50.